New Journal of Physics
The open-access journal for physics

An acoustic spanner and its associated rotational Doppler shift

K D Skeldon, C Wilson, M Edgar and M J Padgett[1]
Department of Physics and Astronomy, University of Glasgow, Glasgow, UK
E-mail: m.padgett@physics.gla.ac.uk

New Journal of Physics **10** (2008) 013018 (9pp)
Received 17 September 2007
Published 21 January 2008
Online at http://www.njp.org/
doi:10.1088/1367-2630/10/1/013018

Abstract. Light carries a spin angular momentum associated with its polarization and an orbital angular momentum arising from its phase cross-section. Sound, being a longitudinal wave, carries no spin component but can carry an orbital component of angular momentum when endowed with an appropriate phase structure. Here, we use a circular array of loudspeakers driven at a common angular frequency ω_s but with an azimuthally changing phase delay to create a sound wave with helical phase fronts described by $\exp(i\ell\theta)$. Such waves are predicted to have an orbital angular momentum to energy ratio of ℓ/ω_s. We confirm this angular momentum content by measuring its transfer to a suspended 60 cm diameter acoustic absorbing tile. The resulting torque on the tile ($\sim 6.1 \times 10^{-6}$ Nm) is measured from observation of the motion for various torsional pendulums. Furthermore, we confirm the helical nature of the acoustic beam by observing the rotational Doppler shift, which results from a rotation between source and observer of angular velocity ω_r. We measure Doppler shifted frequencies of $\omega_s \pm \ell\omega_r$ depending on the direction of relative rotation.

[1] Author to whom correspondence should be addressed.

Contents

1. Introduction

It is now widely recognized that light beams can carry both a spin and orbital angular momentum [1]. The spin angular momentum corresponds to the $\hbar$ spin of individual photons and at a macroscopic level is evident as circular polarization. In 1992, Allen *et al* [2] identified that independently of their polarization state, light beams with an $\exp(\mathrm{i}\ell\theta)$ helical phase structure carried an orbital angular momentum of $\ell\hbar$ per photon. This orbital angular momentum was successfully transferred to a microscopic particle, causing it to spin on the beam axis [3]. Both spin and orbital momenta are directed along the beam axis but whereas the spin component has only two orthogonal states, the orbital component has an unbounded number of orthogonal states, with ℓ taking any integer value. In the case of light, these beams are exemplified by the Laguerre–Gaussian laser modes. However, it is important to appreciate the orbital angular momentum of such beams is not dependent upon the precise form of their radial profile rather upon the helical phase structure alone. Consequently, all beams whether they be Laguerre–Gaussian, Bessel, or arbitrary superpositions of these, carry an orbital angular momentum ℓ. Following the realization of the ease with which these beams can be produced within the laboratory they have featured in many studies of the fundamental properties of light and its applications [4], both classical [5, 6] and quantum [7].

Although described above as quantized in terms of photons, neither the spin nor orbital angular momentum is exclusively a quantum property, both being directly calculable from the cross-products of the EM fields, appropriately integrated over the beam cross-section [8]. However, that waves carry both energy and momentum is not solely a property of electromagnetic radiation, rather a generic property of all waves be they transverse or longitudinal. For both light and sound waves [9], the ratio of the cycled-average momentum flux $\langle\mathbf{P}\rangle$ to the energy flux $\langle\mathbf{E}\rangle$ is the reciprocal of the phase velocity, v_ϕ, of the wave, i.e.

$$\langle\mathbf{P}\rangle/\langle\mathbf{E}\rangle = 1/v_\phi. \tag{1}$$

Sound is no exception to this, meaning that a 1 W sound beam travelling through air, totally absorbed by object, exerts a force of $\approx$0.3 mN. However, in a fluid, sound is a longitudinal rather than transverse wave and is described as a scalar rather than a vector and hence has no polarization. This means that sound beams cannot carry spin angular momentum, but no such restriction exists on their orbital angular momentum content. Indeed the linear [10] and angular [9, 11] momentum content of sound waves have been widely appreciated and compared to their optical counter parts [12, 13].

Within the optical regime, helically phased beams are now routinely made by transformation of a conventional planar wave laser beam using a hologram, i.e. diffractive optic [14, 15]. Acoustic vortices have also been produced but rather than using holographic techniques the required azimuthal phase variation is generated directly using various techniques including optically heated helical surfaces [16] and individually addressed transducers [11]. By analogy with the optical case, or directly [9] the ratio between the cycled-averaged acoustic angular momentum flux $\langle \mathbf{L} \rangle$ and acoustic energy flux $\langle \mathbf{E} \rangle$ is given by

$$\langle \mathbf{L} \rangle / \langle \mathbf{E} \rangle = \ell \lambda / 2\pi v_\phi, \tag{2}$$

where v_ϕ is the phase velocity of the sound in the medium ($\sim$340 m s^{-1} in air at room temperature). Consequently, a helically phased sound wave absorbed by an object, should set the object into rotation: an *acoustic spanner*. We should point out that during preparation of our manuscript, we were alerted to a similar acoustic momentum transfer experiment [17]. We believe that both our own and that experiment are consistent with an interpretation of our results in terms of acoustic angular momentum calculated by equation (2).

Beyond its transfer to matter, another hallmark of helical phase beams is that they are subject to a rotational frequency shift [18]. The rotational frequency shift is an analogous but distinct phenomenon to the better-known linear Doppler shift. Whereas the linear shift is proportional to the velocity between source and observer, the rotational shift is proportional to the product of the angular momentum of the beam and the rotational velocity between source and observer. A frequency shift associated with circular polarization, i.e. the spin angular momentum, was noted as early as 1934 [19]. It has more recently been observed to be proportional to the sum of the spin and orbital angular momentum of a light beam [20]. For a sound wave of angular frequency ω_s, we would therefore expect a frequency shift given by

$$\Delta\omega_\mathrm{s} = \ell \omega_\mathrm{r}, \tag{3}$$

where ω_r is the relative angular velocity between the source and observer.

2. Generating acoustic beams with helical phase

The experimental apparatus to generate an acoustic beam with helical phase is shown in figure 1. We constructed a circular array of 16 loudspeakers, eight of which were used at any given time, each driven by an individual amplifier capable of providing up to 10 W of electrical power. The individual speakers were 6 cm in diameter and the circular array was 52 cm across. The loudspeaker array was itself mounted into the base of a 70 cm diameter cylinder constructed from sound absorbing lead-foam laminate. This laminate absorbs over 90% of the incident sound energy.

The electronics used to drive the loudspeaker array consisted of a signal generator feeding into a phase-shifter circuit providing eight outputs with sequential phases ($\pi/4$ steps). The phase shifter circuit has a logic control line enabling either increasing or decreasing phase as shown in figure 1. This allows for sign reversal of the angular momentum. The outputs from the phase shifter circuit are individually amplified to produce a final set of signals of approximately equal amplitude which are fed to the loudspeakers. The resulting acoustic beam travelling from the loudspeaker array is anticipated to have a helical phase structure described by $\exp(\mathrm{i}\ell\phi)$, where $\ell = \pm 1$ (phase change per axial revolution of the acoustic beam of $\pm 2\pi$) depending on the setting of the logic control. The drive frequency used was around 500 Hz, corresponding to an acoustic wavelength of approximately 68 cm.

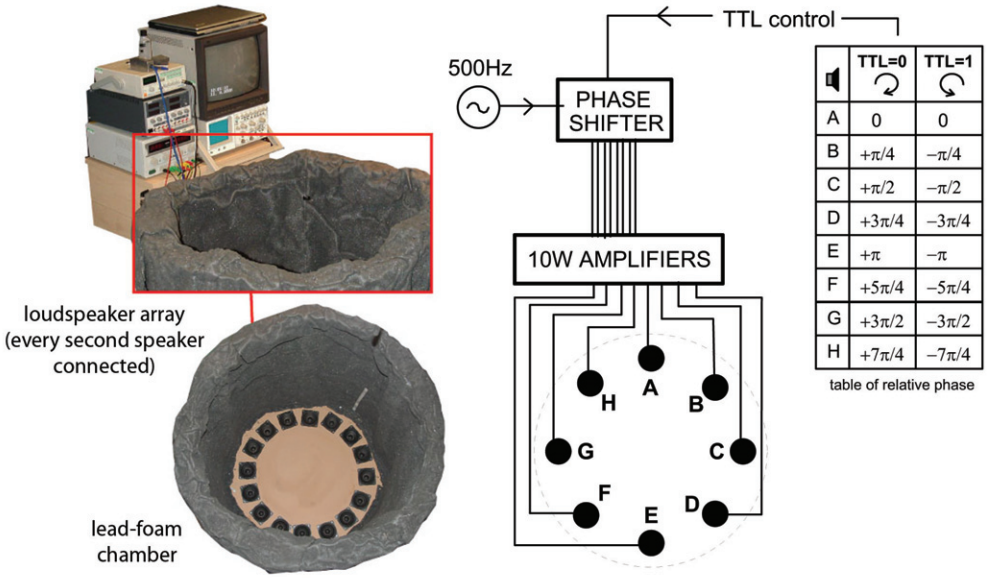

	TTL=0	TTL=1
A	0	0
B	$+\pi/4$	$-\pi/4$
C	$+\pi/2$	$-\pi/2$
D	$+3\pi/4$	$-3\pi/4$
E	$+\pi$	$-\pi$
F	$+5\pi/4$	$-5\pi/4$
G	$+3\pi/2$	$-3\pi/2$
H	$+7\pi/4$	$-7\pi/4$

Figure 1. The experimental system for generating acoustic beams with angular momentum $\ell = \pm 1$. Eight loudspeakers were active in generating the acoustic beam, although twice that number were incorporated to allow for failure or redundancy. The loudspeaker array measured 52 cm in diameter and was placed at the base of a containment cylinder of lead-foam walls $\sim$70 cm diameter.

3. Acoustic spanner

The acoustic spanner set-up is shown in figure 2(a). The acoustic beam is directed upwards toward a 60 cm diameter tile, manufactured from acoustic absorbing foam suspended from a thin steel wire above the speaker array.

The diameter of the speaker array is of the order of the acoustic wavelength, consequently one might expect that the resulting sound beam diverges with the individual speakers acting as point sources, albeit with the walls of the containment cylinder having some effect on the propagating field. It is the interference between these speakers that establishes a helically phased beam with a minimum of intensity on the beam axis. To maximize the momentum transfer between these speakers and the tile, we position the tile approximately 15 cm above the speaker array, i.e. in the near-field. The sound field at this point has an annular intensity profile, suggestive of a Laguerre–Gaussian mode. Closer examination would show that this resemblance is only an approximation, but it is imperative to appreciate that the orbital angular momentum to energy ratio is solely a function of the helical phase fronts and therefore is unchanged between the near and far fields. To further probe the acoustic beam, we have made radial measurements across the planes of interest in our experiment and found the sound pattern to be remarkably consistent, as detailed in figure 4.

In order to establish a reproducible set of observations, we made measurements with various suspension wire radii and lengths. Observations were recorded using a DV camera pointing towards the circular tile allowing its motion to be compared against an angular scale overlaid on a remote monitor. This also facilitated the effective isolation of the experiment

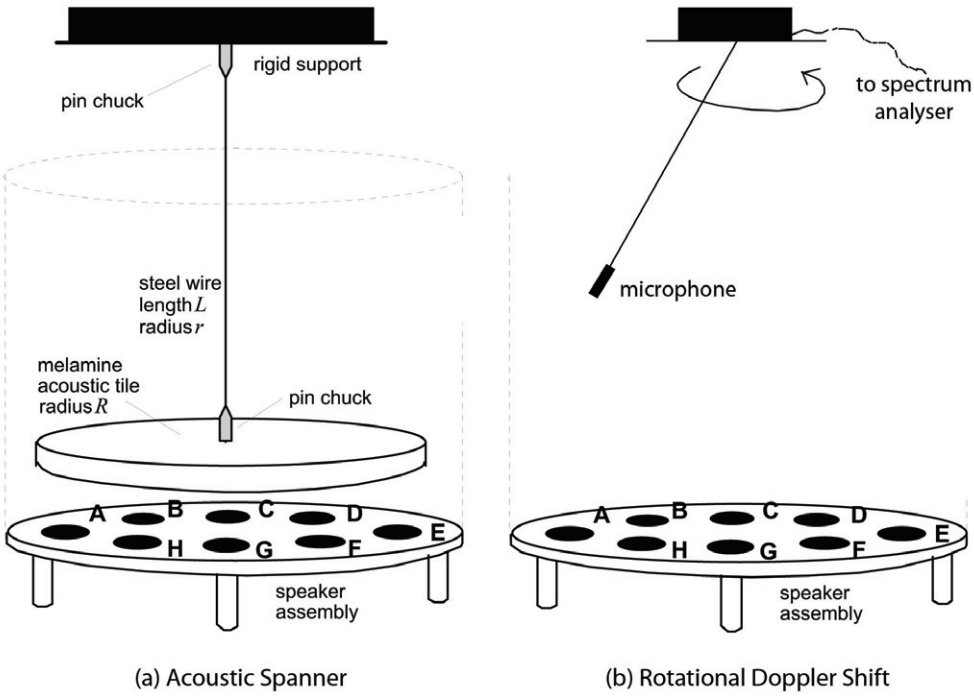

Figure 2. The set-up to demonstrate (a) the acoustic spanner and (b) the rotational Doppler shift. The acoustic tile measured 60 cm in diameter and was suspended approximately 15 cm above the loudspeakers. For the rotational Doppler experiment, the microphone was swept in a circular arc approximately 80 cm above the loudspeaker array.

during operation, reducing disturbance and enabling the experimental data-set to be analysed later against the DV-tape digital time-stamp. The logic control of the phase shifter circuit was used to remotely change the angular momentum direction while recording results.

Starting with the tile initially at rest, the sound field was switched on and the resulting angular motion observed. The differential equation governing the motion of the torsional pendulum is

$$\Gamma_s = I\ddot{\theta} + \gamma\dot{\theta} + k\theta, \tag{4}$$

where θ is the angular displacement, Γ_s is the torque exerted on the tile by the incident acoustic beam, I is the moment of inertia of the tile ($0.022\,\mathrm{kg\,m^2}$), γ is the viscous damping coefficient and k is the torsional stiffness constant of the pendulum. The motion is that of an under-damped torsional pendulum. In figure 3, we show an experimental data-set of the motion overlayed with that predicted by equation (4). The various parameters indicated on the graph are all directly measurable from careful observation of the angular motion of the tile. In particular, by using the initial acceleration α_i, the period of the oscillatory motion T and the final angle of rest of the tile θ_{max}, we can deduce Γ_s by alternative methods. Firstly, the initial angular acceleration can be used with I to yield

$$\Gamma_s = I\alpha_i. \tag{5}$$

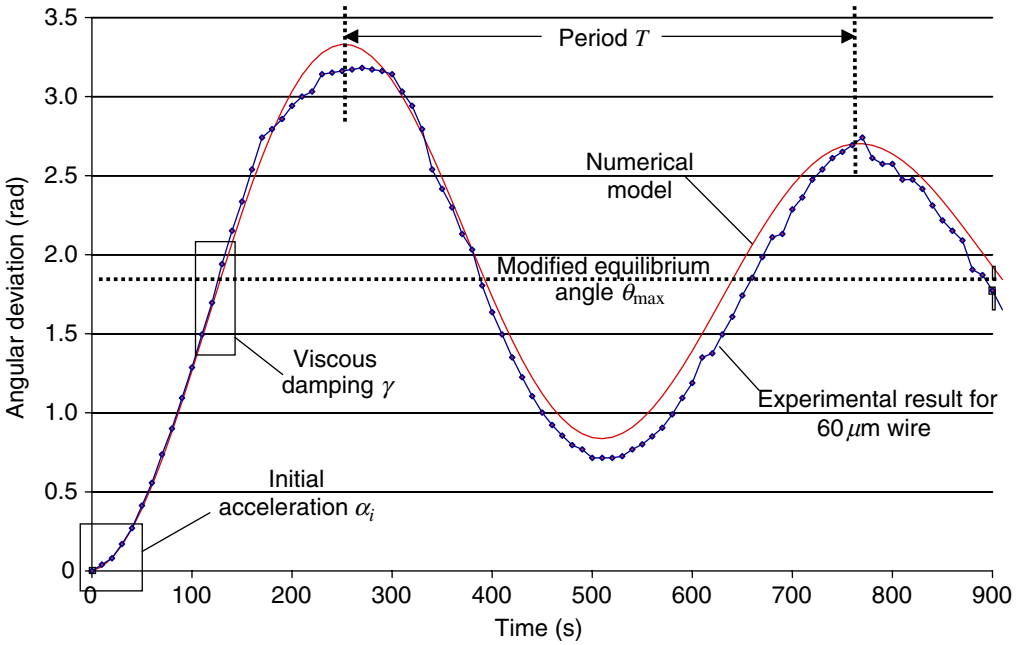

Figure 3. Comparison of the motion of the pendulum calculated from the equation of motion and the observed angular displacement. The parameters for damping and stiffness constant are deduced from observation and the resulting agreement between predicted and observed motion is good. Measurements of torque can be deduced from α_i ($\Gamma_s = I\alpha_i$) or T and θ_{max} ($\Gamma_s = 4\pi^2 I\theta_{max}/T^2$).

Secondly, by considering the pendulum to be undergoing simple harmonic motion with period $T = 2\pi\sqrt{I/k}$, we can deduce the torsional stiffness constant k. Thereafter, we can use this value for k along with θ_{max} to give

$$\Gamma_s = k\theta_{max} = \frac{4\pi^2 I}{T^2}\theta_{max}. \tag{6}$$

Finally, these values for torque can be compared with an estimation of the acoustic torque based on the acoustic power incident on the tile.

The results presented in table 1 show measurements made for two wire radii 50 and 60 μm. We note that in the case of the 50 μm wire, θ_{max} is 5.8 radians, is close to one full rotation of the acoustic tile. The torque values calculated from the initial acceleration and modified equilibrium position are shown. We have averaged results over $\ell = \pm 1$ for each suspension configuration. Given the uncertainties in both measurement and system parameters, these values of torque shown in table 1 are reasonably consistent with each other. Assuming each of these to be free of systematic error, we obtain a best estimate of the measured torque to be $6.1 \pm 0.8 \times 10^{-6}$ Nm, an answer which is itself statistically compatible with the individual measurements.

This observed value can be compared to that estimated from the acoustic power from equation (2). The acoustic power is itself estimated from the measured electrical power to the speakers taken along with a stated audio efficiency of 0.5%. We also averaged measurements of the typical sound pressure level at the plane of the tile and found the two approaches to agree within the experimental uncertainty of the overall system. Having estimated the acoustic energy, the resulting torque depends upon the absorption of the tile material, which is based

Table 1. Summary of acoustic spanner results. Torque values are shown for the methods described in the text, using the initial and long-term parts of the observed motion. Ideally, for a given acoustic set-up, we would expect the torque to be independent of suspension wire radius and comparable to the value measured from the properties of the acoustic beam (estimated to be 6.4×10^{-6} Nm).

r (μm)	L (m)	θ_{max} (rad)	Γ (Nm) based on α_i	Γ (Nm) based on θ_{max}, T
50	1.89	5.80	$5.6 \pm 1.4 \times 10^{-6}$	$6.0 \pm 0.6 \times 10^{-6}$
60	1.22	1.95	$4.5 \pm 1.8 \times 10^{-6}$	$6.5 \pm 0.7 \times 10^{-6}$

on information given by the manufacturer and is estimated to be 30% for our configuration, a figure confirmed by our own reflection/transmission measurements. Using this approach acoustic torque is estimated to be $\Gamma_s = 6.4 \times 10^{-6}$ Nm, which within the experimental errors agrees with our observations.

A video of the acoustic spanner can be seen in *spanner.mov* (available from stacks.iop.org/njp/10/013018/mmedia) where the motion for the 60 μm wire is shown speeded up by a factor of $\sim \times 20$. Thinner and longer wires resulted in an increased rotation, with θ_{max} exceeding one complete revolution, albeit with some thermal instability.

4. Rotational Doppler shift

The experiment described in the previous section has demonstrated the acoustic angular momentum produced by our loudspeaker array.

Central to the analysis of that section is the assumption that the speaker array generates a helically phase beam described by $\exp(i\ell\theta)$, and that this phase structure is not compromised by any residual reflection from the containment cylinder. We check this assumption by considering another, independent, property of helically phase beams; namely the rotational Doppler effect experienced by an observer rotating around the axis the beam. The basic experiment is depicted in figure 2(b). For a frequency ω_s fed into the loudspeaker electronics, we measure ω_s from a static microphone positioned anywhere in the sound field, albeit with changing phase depending on the position across the helical phase front. In the particular case when the microphone is swept in a circular path in a plane parallel to the speaker array at an angular velocity ω_r, we observe a rotational Doppler shift which results in a modified frequency $\omega_s \pm \ell\omega_r$. The direction of rotation determines whether the Doppler shift is upwards or downwards in frequency. Note that the situation here contrasts with those where rotational motion can lead to a linear Doppler shift. Fundamentally, the Doppler shift described here involves no change of distance between the observer and the source therefore no linear component of the Doppler shift can exist.

To show the rotational Doppler shift experimentally, we arranged for a microphone to be rotated around the beam axis and the signal to be recorded with a Stanford FFT Analyser (model SR780). The microphone was swept in a circular arc with size roughly equivalent to that of the speaker array and around 80 cm above the speakers. In figure 4, we show a typical traverse scan across the plane containing the circular arc swept out by the microphone. This shows the sound field to possess a central minimum as would be expected for the $\ell = 1$ mode generated by the speaker array. In figure 5, we show an example of Doppler shifted frequency peaks

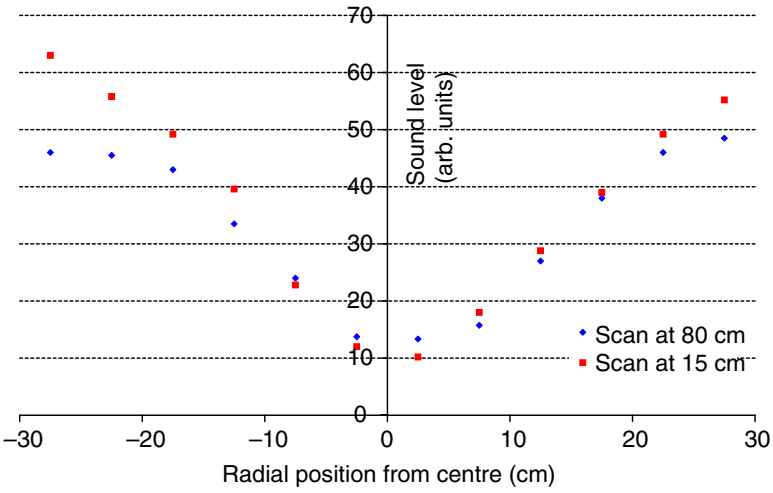

Figure 4. Measurements of the sound level across the diameter of the containment cylinder at the position of the acoustic tile (15 cm height above the loudspeakers) and the plane where Doppler results were taken (∼80 cm above the loudspeakers). Each trace represents an average of several traverse scans with a roaming microphone.

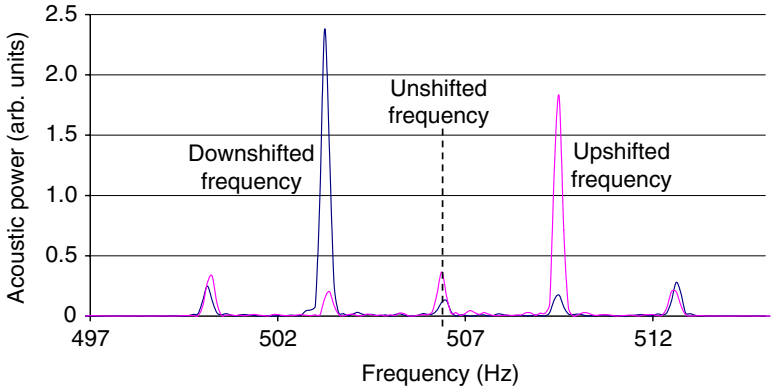

Figure 5. Results of the rotational Doppler effect measured with a spinning microphone. The frequency offset in Hz, Δf_r, is equal to the revolutions per second made by the microphone relative to the source (or $\omega_r/2\pi$, where ω_r is the relative angular velocity). The downshifted frequency corresponds to the case when the microphone is rotated in the direction of increasing phase of the helical phase front.

corresponding to both rotation directions of the microphone. The dominant spectral component of the sound field clearly moves either above or below the baseline value depending on whether the microphone is rotated in the direction of increasing phase or decreasing phase of the helical phase front. Slight variations in the volume of successive speakers as the microphone passes around the sound field give azimuthal variation in the acoustic energy. In terms of the constituent modes this corresponds to a superposition of different ℓ values. Consequently one expects, and indeed observes weak sidebands both above and below our shifted frequency. We note that these

are small and reasonably symmetric about the centre frequency suggesting that the average ℓ value is not significantly perturbed from $\ell = \pm 1$.

In both cases the dominant peak occurs at the Doppler shifted frequency we would expect from equation (3).

5. Conclusion

We have demonstrated angular momentum transfer between an acoustic beam with helical phase ($\ell = \pm 1$) and a suspended tile. Results show good self-consistency between the motion of the tile and the suspension parameters. We have confirmed the helical phase structure of the acoustic beam by measuring the Doppler shift for a rotating observer.

Acknowledgments

K D Skeldon acknowledges the support of the DTI, the NERC and NESTA while CW was supported by a University of Glasgow vacation grant. We would also like to thank Karen Volke and her colleagues for useful discussions in the preparation of our manuscript.

References

[1] Allen L, Padgett M J and Babiker M 1999 *Prog. Opt.* **39** 291–372
[2] Allen L, Beijersbergen M W, Spreeuw R J C and Woerdman J P 1992 *Phys. Rev.* A **45** 8185–9
[3] He H, Friese M E J, Heckenberg N R and Rubinsztein-Dunlop H 1995 *Phys. Rev. Lett.* **75** 826–9
[4] Allen L, Barnett S M and Padgett M J 2003 *Optical Angular Momentum* (Bristol: Institute of Physics Publishing)
[5] Padgett M J and Allen L 2000 *Contemp. Phys.* **41** 275–85
[6] Padgett M, Courtial J and Allen L 2004 *Phys. Today* **57** 35–40
[7] Molina-Terriza G, Torres J P and Torner L 2007 *Nat. Phys.* **3** 305–10
[8] O'Neil A T, MacVicar I, Allen L and Padgett M J 2002 *Phys. Rev. Lett.* **88** 053601
[9] Lekner J 2006 *J. Acoust. Soc. Am.* **120** 3475–7
[10] McIntyre M E 1981 *J. Fluid Mech.* **106** 331–47
[11] Hefner B T and Marston P L 1999 *J. Acoust. Soc. Am.* **106** 3313–6
[12] Thomas J L and Marchiano R 2003 *Phys. Rev. Lett.* **91** 244302
[13] Marchiano R and Thomas J L 2005 *Phys. Rev.* E **71** 066616
[14] Bazenhov V Y, Vasnetsov M V and Soskin M S 1990 *JETP Lett.* **52** 429–31
[15] Heckenberg N R, McDuff R, Smith C P and White A G 1992 *Opt. Lett.* **17** 221–3
[16] Gspan S, Meyer A, Bernet S and Ritsch-Marte M 2004 *J. Acoust. Soc. Am.* **115** 1142–6
[17] Volke-Sepulveda K P, Orozco-Santillan A, Vasquez-Arzola A, Hernandez-Candia N and Jauregui R 2007 *Proc. SPIE* (Technical Program p 61)
[18] Garetz BA 1981 *J. Opt. Soc. Am.* **71** 609–11
[19] Atkinson RDE 1934 *Phys. Rev.* **47** 623–7
[20] Courtial J, Robertson D A, Dholakia K, Allen L and Padgett M J 1998 *Phys. Rev. Lett.* **81** 4828–30